Molecular Cell
Article

Distinct and Combinatorial Functions of Jmjd2b/Kdm4b and Jmjd2c/Kdm4c in Mouse Embryonic Stem Cell Identity

Partha Pratim Das,[1,10] Zhen Shao,[1,10] Semir Beyaz,[1] Eftychia Apostolou,[3,4] Luca Pinello,[5] Alejandro De Los Angeles,[1] Kassandra O'Brien,[1] Jennifer Marino Atsma,[1,9] Yuko Fujiwara,[1] Minh Nguyen,[1] Damir Ljuboja,[1,8] Guoji Guo,[1] Andrew Woo,[7] Guo-Cheng Yuan,[5] Tamer Onder,[1,6] George Daley,[1,2,3] Konrad Hochedlinger,[2,3,4] Jonghwan Kim,[1,8] and Stuart H. Orkin[1,2,*]

[1]Department of Pediatric Oncology, Dana-Farber Cancer Institute and Division of Hematology/Oncology, Boston Children's Hospital, Harvard Stem Cell Institute, Harvard Medical School, Boston, MA 02115, USA
[2]Howard Hughes Medical Institute, Boston, MA 02115, USA
[3]Department of Stem Cell and Regenerative Biology, Harvard University and Harvard Medical School, 7 Divinity Avenue, Cambridge, MA 02138, USA
[4]Center for Regenerative Medicine, Massachusetts General Hospital Cancer Center, Boston, MA 02114, USA
[5]Department of Biostatistics and Computational Biology, Dana-Farber Cancer Institute, Harvard School of Public Health, Boston, MA 02115, USA
[6]School of Medicine, Koç University, Rumelifeneri Yolu, Sariyer 34450, Istanbul, Turkey
[7]Western Australian Institute for Medical Research, Royal Perth Hospital and School of Medicine and Pharmacology, The University of Western Australia, Nedlands, WA 6009, Australia
[8]Present address: Section of Molecular Cell and Developmental Biology, Institute for Cellular and Molecular Biology, University of Texas at Austin, Austin, TX 78712, USA
[9]Present address: Abbott Bioresearch Center, 100 Research Drive, Worcester, MA 01605, USA
[10]These authors contributed equally to this work
*Correspondence: stuart_orkin@dfci.harvard.edu
http://dx.doi.org/10.1016/j.molcel.2013.11.011

SUMMARY

Self-renewal and pluripotency of embryonic stem cells (ESCs) are established by multiple regulatory pathways operating at several levels. The roles of histone demethylases (HDMs) in these programs are incompletely defined. We conducted a functional RNAi screen for HDMs and identified five potential HDMs essential for mouse ESC identity. In-depth analyses demonstrate that the closely related HDMs Jmjd2b and Jmjd2c are necessary for self-renewal of ESCs and induced pluripotent stem cell generation. Genome-wide occupancy studies reveal that Jmjd2b unique, Jmjd2c unique, and Jmjd2b-Jmjd2c common target sites belong to functionally separable Core, Polycomb repressive complex (PRC), and Myc regulatory modules, respectively. Jmjd2b and Nanog act through an interconnected regulatory loop, whereas Jmjd2c assists PRC2 in transcriptional repression. Thus, two HDMs of the same subclass exhibit distinct and combinatorial functions in control of the ESC state. Such complexity of HDM function reveals an aspect of multilayered transcriptional control.

INTRODUCTION

Embryonic stem cells (ESCs) are capable of indefinite self-renewal and differentiation into all lineages. Somatic cell reprogramming to induced pluripotent stem cells (iPSCs) by defined factors has greatly improved prospects for cellular therapies (Takahashi and Yamanaka, 2006; Cherry and Daley, 2012). Although much has been learned, the components that establish and maintain ESC identity are incompletely defined.

ESC identity is maintained by activation of ESC-specific genes and repression of lineage-specific developmental genes. This balance of gene expression is maintained through crosstalk between essential transcription factors (TFs) and chromatin regulators (Orkin and Hochedlinger, 2011; Young, 2011). Extensive studies of protein-protein and protein-DNA interactions have revealed distinct ESC regulatory modules, termed Core, Myc, and Polycomb, that are essential for the entire ESC regulatory network (Chen et al., 2008; Kim et al., 2010). The Core module is composed of canonical ESC factors (Oct4, Sox2, and Nanog) and their associated partners, which positively regulate ESC-specific genes and repress lineage-specific genes (Kim et al., 2010; Young, 2011). The Myc module, consisting of cMyc and associated factors, is also transcriptionally active. However, the Myc module is functionally separable from the Core module and is activated earlier than the Core module during iPSC generation at the partial iPSC stage (Sridharan et al., 2009; Soufi et al., 2012). The Polycomb repressive complex (PRC) module, composed of PRC1 and PRC2 components, functions in repression of lineage-specific genes (Boyer et al., 2006; Kim et al., 2010; Margueron and Reinberg, 2011).

Various approaches have implicated the role of chromatin regulators in self-renewal of ESCs (Fazzio et al., 2008; Hu et al., 2009; Kagey et al., 2010). Histone demethylases (HDMs) are histone-modifying enzymes, which have an opposing biochemical

function to histone methyltransferases (HMTs). HDMs are required for normal development and are implicated in pathologic states including cancers (Pedersen and Helin, 2010). HDMs are divided into two broad classes, FAD-dependent amine oxidases (Lsd1/Kdm1) and Fe(II)- and α-ketoglutarate-dependent JmjC domain-containing HDMs (Mosammaparast and Shi, 2010). The JmjC domain-containing HDMs have a conserved catalytic triad (H, D/E, and H), which catalyzes lysine demethylation of histones through an oxidative reaction that requires Fe(II) and α-ketoglutarate as cofactors. JmjC domain-containing HDMs are further subclassified based on their sequence homology, domains, and substrate specificity (Agger et al., 2008; Pedersen and Helin, 2010). Studies have proposed roles for Jmjd1a, Jmjd2c, and Jarid1b/Kdm5b in ESC self-renewal (Loh et al., 2007; Xie et al., 2011). However, roles of other HDMs in ESCs remain unknown.

Here, we conducted a functional RNAi screen against all annotated HDMs and identified five candidate HDMs essential for mouse ESC (mESC) identity. To gain mechanistic insight, we chose two closely related HDMs, Jmjd2b/Kdm4b and Jmjd2c/Kdm4c, belonging to the same subclass (HDMs for H3K9me2/me3 and H3K36me2/me3) for in-depth analysis. In addition to their requirement in ESCs, both HDMs are required for efficient somatic cell reprogramming. Although depletion of either HDM generates a similar differentiation phenotype, chromatin occupancy studies reveal both unique and common target sites. Jmjd2b unique, Jmjd2b-Jmjd2c common, and Jmjd2c unique targets partition to the Core, Myc, and PRC regulatory modules of the overall ESC network, respectively. Specifically, we show that Jmjd2b and Nanog act through an interconnected regulatory loop, whereas Jmjd2c assists PRC2 in full repression at poised and repressed target genes. The dedicated and combinatorial relationships between these two related HDMs reveal an unsuspected level of complexity in how HDMs participate in transcriptional control.

RESULTS

Functional RNAi Screens Reveal Candidate HDMs for mESC Identity

Most HDMs are expressed in mESCs (Figure S1A available online). To identify HDMs required for maintenance of the ESC state, we performed a functional RNAi screen. We used five different shRNA lentiviral constructs to knock down each of 20 HDMs in mESCs. The screen was scored in terms of alterations of "ESC growth phenotype" and "colony morphology" (Figure 1A; Figure S1B; Table S1). Normally, ESCs grow as spherical three-dimensional colonies. Upon depletion of a number of the candidate HDMs, cells exhibited flattened morphology and grew as a monolayer with reduced cell-cell contacts (Figure S1B), which we term a "differentiation" phenotype. A spectrum of differentiation phenotypes from mild to severe was observed (Figure S1B; Table S1). For each candidate HDM, we scored the phenotype from at least the two best individual shRNAs. Two secondary screens were performed for validation. All three screens reproduced the original phenotypes (Table S1).

Our functional RNAi screen identified five candidate HDMs, namely Jmjd1a (Kdm3a), Jmjd2b (Kdm4b), Jmjd2c (Kdm4c), Utx (Kdm6a), and Jmjd6. Among these, Jmjd1a (Kdm3a) and Jmjd2c (Kdm4c) were identified previously as having a role in self-renewal of mouse ESCs (Loh et al., 2007). Jmjd1a, Jmjd2b, Jmjd2c, and Jmjd6 knockdown showed moderate to severe differentiation phenotypes, whereas knockdown of Utx showed a more subtle phenotype (Figure S1B; Table S1). Further analyses were performed for the candidate HDMs. Alkaline phosphatase staining typical of pluripotent ESCs was reduced upon knockdown of candidate HDMs compared to controls (Anti-GFP and Empty) (Figure 1B). Pluripotency marker SSEA-1 expression was also reduced significantly upon knockdown (Figure 1C). We validated each by western blotting (Figure S1C), and noted general correlation of knockdown efficiency with the extent of differentiation. mRNA expression and protein levels of all five candidate HDMs were reduced upon ESC differentiation (Figures 1D and 1E). Additionally, these candidate HDMs were highly expressed in mESCs compared to mouse embryonic fibroblasts (Figure S1D), consistent with crucial roles in mESC identity.

Both Jmjd2b/Kdm4b and Jmjd2c/Kdm4c Are Required for ESC Identity and Efficient Somatic Cell Reprogramming/iPSC Generation

We selected two closely related candidate HDMs of the same subclass, Jmjd2b and Jmjd2c, for in-depth study (Agger et al., 2008). As depletion of either leads to an apparently similar differentiation phenotype, we suspected that their comparison might uncover insights into their nonredundant roles and possibly their relationship to each other.

We first determined that Jmjd2b and Jmjd2c restore the normal ESC growth and colony morphology in *Jmjd2b*-deficient and *Jmjd2c*-deficient ESCs (Figure S1E). Indeed, full-length Jmjd2b and Jmjd2c restored the normal ESC growth phenotype, ESC colony morphology, and also SSEA-1 expression (Figures S1F and S1G). However, catalytic domain (JmjC)-containing Jmjd2b and Jmjd2c (1–333 aa) and catalytic mutants (JmjC domain-containing catalytic triad [H, D/E, and H]) of Jmjd2b and Jmjd2c achieved only partial rescue (Figures S1F and S1G), suggesting that the full length of Jmjd2b and Jmjd2c, as well as their catalytic residues, is required for self-renewal of mESCs.

Next, we tested the role of Jmjd2b and Jmjd2c in somatic reprogramming. Depletion of Jmjd2b and Jmjd2c showed reduced numbers of iPSC colonies compared to control knockdown, as scored by colony morphology and SSEA-1-positive colonies (Figure 1F), which is reminiscent of the effects of knockdown of all H3K9 demethylases (Chen et al., 2013). Taken as a whole, the functional assay demonstrates that Jmjd2b and Jmjd2c are required for efficient somatic reprogramming induced by Oct4-Sox2-Kl4-Myc and establishment of the ESC-like state.

Jmjd2b/Kdm4b and Jmjd2c/Kdm4c Are Required for Self-Renewal of mESCs

We next conducted gene expression profiling upon depletion of Jmjd2b and Jmjd2c compared to control (Anti-GFP) knockdown. Gene expression profiling revealed that 1,787 genes were differentially expressed by >2-fold upon depletion of Jmjd2b and Jmjd2c (Figure 2A, left; Table S3). The gene cluster down-regulated upon knockdown displayed higher expression in

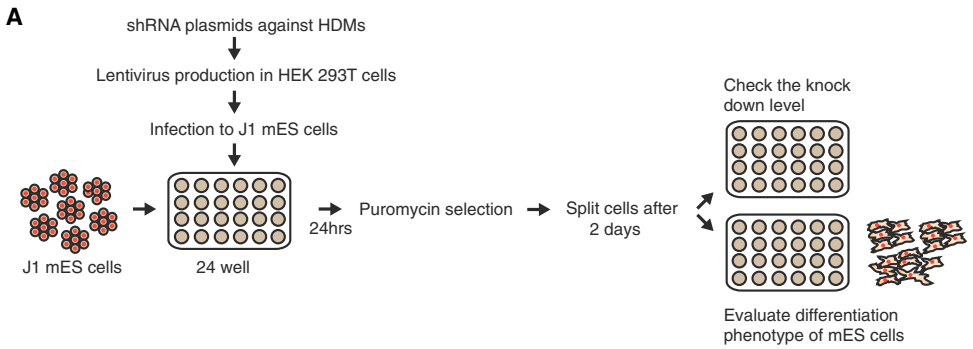

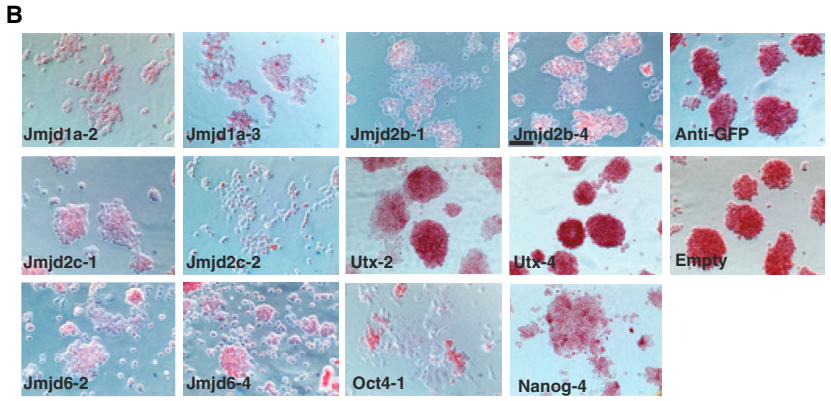

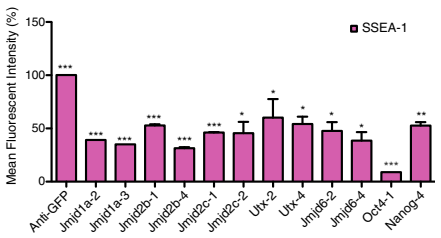

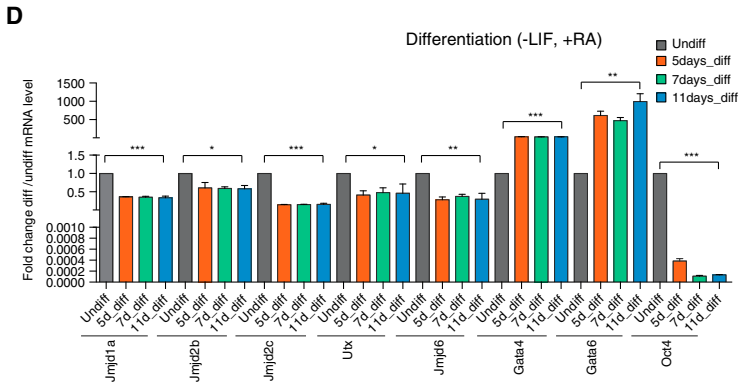

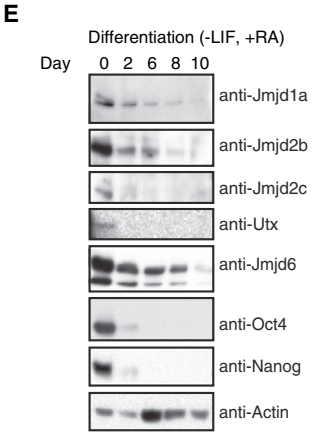

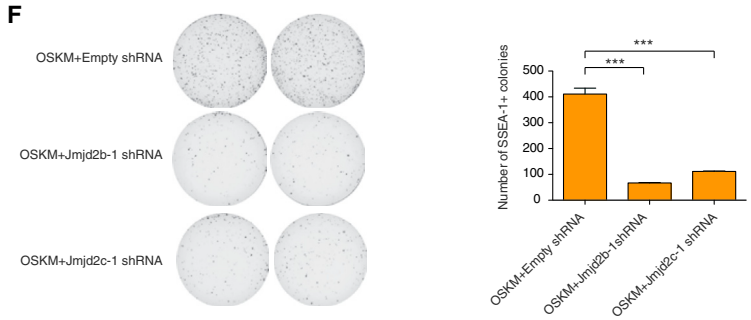

(legend on next page)

undifferentiated ESCs compared to differentiated ESCs; conversely, the gene cluster upregulated upon knockdown showed reduced expression in undifferentiated ESCs (Figure 2A, right; Figure S2A).

Expression of individual ESC-specific and lineage-specific genes from Jmjd2b and Jmjd2c depleted cells revealed reduced ESC-specific gene expression and enhanced expression of differentiation genes (Figures 2C and 2D; Figures S2B and S2C). We observed modest downregulation of ESC-specific genes, including Nanog, Esrrb, Klf4, and Tbx3, in Jmjd2b- or Jmjd2c-depleted cells. In addition, specific knockdown of Jmjd2b and Jmjd2c did not affect expression of other HDMs of the same subclass. We observed upregulation of several lineage-specific genes upon depletion of Jmjd2b or Jmjd2c, such as Brachyury (T), Pitx2, Fgf8, Wnt, and Fgf5 for mesoendoderm/mesoderm, Otx2, Nestin, Pax6, Fabp7, and Zic1 for ectoderm/neuroectoderm, and Cdx2 for trophoectoderm (Figures 2C and 2D; Figures S2B and S2C).

Gene ontology (GO) and Ingenuity Pathway Analysis (IPA) of the upregulated genes revealed significant enrichment for several developmental processes and related signaling pathways, whereas the downregulated genes correlated with several metabolic pathways, including glycolysis and gluconeogenesis (Figures S2D and S2E; Table S5). Furthermore, gene set enrichment analyses (GSEAs) demonstrated that Jmjd2b and Jmjd2c depletion significantly repressed the "undifferentiated" ESC state and enhanced the "differentiation" state (Figures 2E and 2F; Figure S2F; Table S4), including changes in several developmental signaling pathway gene sets (Figure S2G). In these analyses, we observed a similar overall pattern of global gene expression upon depletion of Jmjd2b or Jmjd2c. However, the total number of differentially expressed genes differed between Jmjd2b and Jmjd2c knockdown cells (Figure 2B), raising the possibility that Jmjd2b and Jmjd2c function through common and distinct mechanisms in self-renewal of ESCs.

Differential Distribution of Genome-wide Targets of Jmjd2b/Kdm4b and Jmjd2c/Kdm4c in mESCs

To dissect mechanisms by which Jmjd2b and Jmjd2c function, we determined their genome-wide DNA chromatin occupancy using chromatin immunoprecipitation sequencing (ChIP-seq). Due to the lack of suitable antibodies, we generated biotinylated versions of Jmjd2b and Jmjd2c in mESCs (Figures S3A and S3B) and performed in vivo biotinylation-mediated ChIP-seq (Bio-ChIP-seq) (Kim et al., 2008, 2009, 2010); 16,807 and 18,025 significantly enriched binding peaks were identified for Jmjd2b and Jmjd2c, respectively (Table S6). Despite their close relationship, we observed differential genome-wide distribution of Jmjd2b and Jmjd2c peaks. Jmjd2b peaks are distributed to the promoter (~40%), intergenic (~32%), and gene body regions (~28%), whereas Jmjd2c mostly occupies promoter regions (~70%) compared to ~20% binding at intergenic and ~11% at gene body regions (Figure 3A). Jmjd2b and Jmjd2c share ~40% common peaks/targets (Figure 3B). We further classified targets as "Jmjd2b-Jmjd2c common," "Jmjd2b unique," and "Jmjd2c unique" (Figure 3B). Interestingly, the majority of Jmjd2b-Jmjd2c common and Jmjd2c unique targets are distributed at promoter regions (~77% and ~65%, respectively), whereas Jmjd2b unique targets predominantly localized to gene body regions (~42%) and intergenic regions (~48%), and only ~10% to promoter regions (Figure 3B).

Next, we compared the occupancy of Jmjd2b and Jmjd2c with four metagenes, groups of genes with correlated expression (high, moderate, low, and very low) in mESCs. Further analyses showed that the majority of Jmjd2b-Jmjd2c common targets and Jmjd2b unique targets are occupied at promoters and distal regions, respectively, and correspond to highly expressed genes, whereas the majority of Jmjd2c unique targets are occupied at the promoters of moderately, as well as lowly, expressed genes (Figure S3C). These initial observations reveal distinct distributions and functions of Jmjd2b and Jmjd2c in mESCs.

Jmjd2b/Kdm4b Unique, Jmjd2c/Kdm4c Unique, and Jmjd2b/Kdm4b-Jmjd2c/Kdm4c Common Target Regions Belong to Different Regulatory Modules of mESCs

To explore the significance of Jmjd2b-Jmjd2c common, Jmjd2b unique, and Jmjd2c unique targets, we correlated occupancy maps with histone marks (H3K4me1/3, H3K9me2/me3, H3K27me3, H3K36me2/me3, and H3K27ac), components of the PRC2 complex (Ezh2 and Suz12), ESC-related TFs (Oct4, Nanog, Sox2, and Klf4), and associated transcription factors and chromatin regulators (cMyc, E2F1, p300, Med1, and Med12). As the majority of the Jmjd2b unique targets mapped to "nonpromoter" regions (Figure 3B), we generated ChIP-seq intensity heat maps around the summit of all three peak sets, which were further classified into "promoter" and "distal" regions. We found that the three target classes associated with

Figure 1. Functional RNAi Screens Reveal Candidate HDMs for mESC Identity

(A) Schematic diagram representing the outline of the RNAi screen.

(B) Alkaline phosphatase staining of mESCs upon knockdown of candidate HDMs. The scale bar represents 20 μm.

(C) SSEA-1 staining of mESCs upon knockdown of candidate HDMs. SSEA-1-positive cells were quantified through fluorescence-activated cell sorting, and the percentage of mean fluorescent intensity of candidate HDMs is represented. Data are represented as mean ± SEM; n = 3; p values were calculated using t test; ***$p < 0.0001$, **$p < 0.001$, *$p < 0.01$.

(D) Real-time PCR analyses of candidate HDMs at different time points during ESC differentiation. mRNA expression was normalized by actin, and expression levels are shown in differentiated ESCs relative to undifferentiated ESCs for each gene. Data are represented as mean ± SEM; n = 3; p values were calculated using t test; ***$p < 0.0001$, **$p < 0.001$, *$p < 0.01$.

(E) Western blot analyses of candidate HDMs at different time points during ESC differentiation.

(F) SSEA-1 staining of iPSC colonies from Empty (control) and Jmjd2b and Jmjd2c knockdown cells. Data are represented as mean ± SEM; n = 3; p values were calculated using t test; ***$p < 0.0001$.

See also Figure S1.

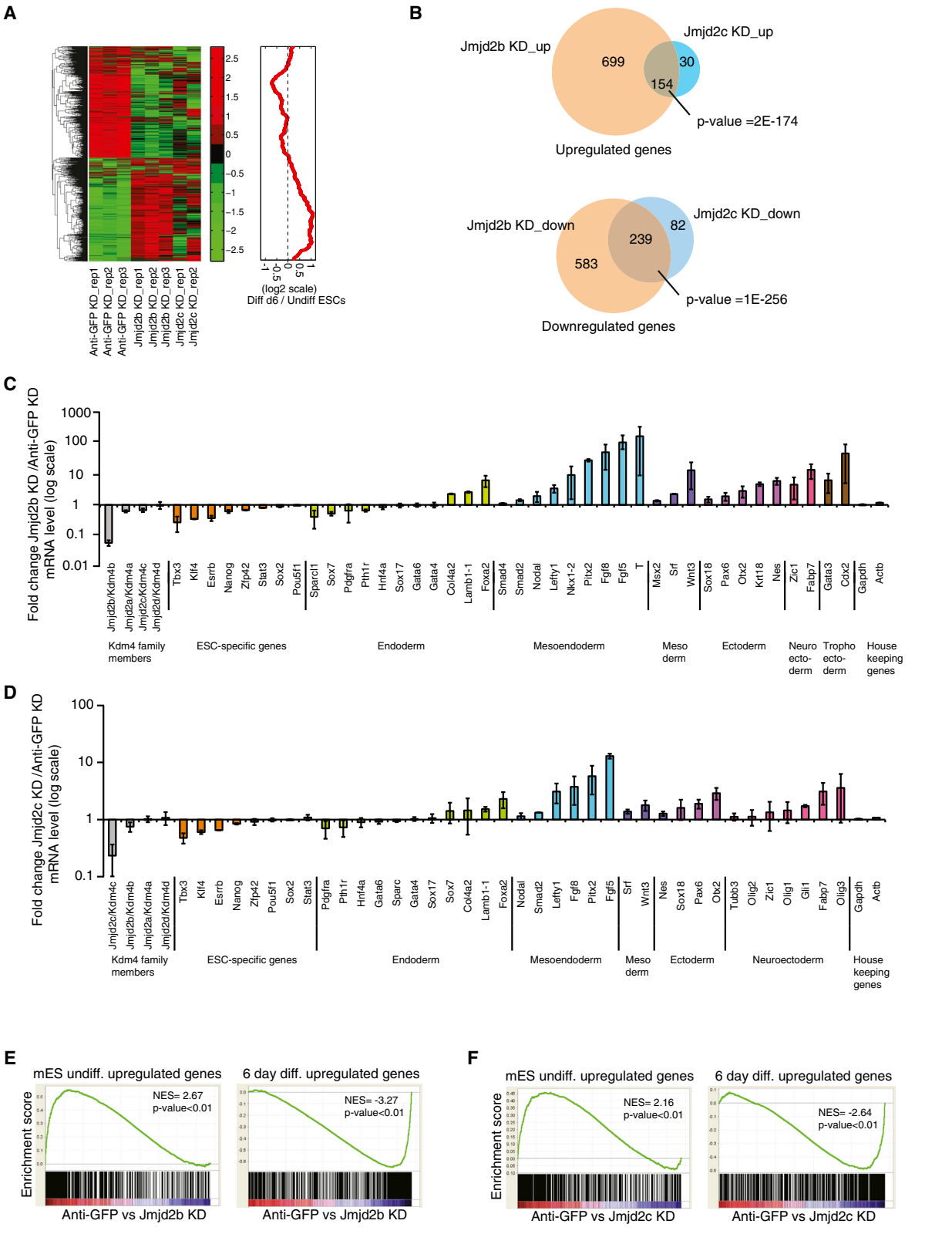

(legend on next page)

different histone marks and transcription factors. Jmjd2c unique targets strongly overlapped with bivalent marks (both H3K4me3 and H3K27me3 marks), and also with components of the PRC2 complex (Ezh2 and Suz12) at promoter and distal target loci (Figure 3C; Figure S3E). Approximately 80% of Ezh2 and Suz12 targets overlapped with Jmjd2c targets genome-wide (Figure 3D). Additionally, H3K36me3 and RNA Pol II occupancy was reduced at Jmjd2c unique promoter and distal target loci (Figure 3C; Figure S3E), suggesting that the majority of Jmjd2c unique targets are poised or repressed. In contrast, Jmjd2b-Jmjd2c common and Jmjd2b unique targets showed reduced occupancy of H3K27me3, Ezh2, and Suz12 and gain of H3K4me3, H3K36me3, and RNA Pol II occupancy both at promoters and distal target loci (Figure 3C; Figure S3E), indicating that these targets are transcriptionally active. Notably, we found that binding of ESC-Core transcription factors Nanog and Sox2 but not Oct4 was strongly biased toward Jmjd2b unique targets rather than the other two peak sets at both promoter and distal regions (Figures 3E and 3F). This was further supported by peak overlap analysis (Figure 3G). Nonetheless, H3K27ac, H3K4me1, p300, mediator (Med1, Med12), and Klf4 binding sites overlapped with both Jmjd2b unique and Jmjd2b-Jmjd2c common targets, and targets of cMyc and its associated factor E2f1 showed significant overlap with Jmjd2b-Jmjd2c common target genes at promoter and distal target loci (Figures 3E–3G).

For a global view of Jmjd2b unique, Jmjd2c unique, and Jmjd2b-Jmjd2c common targets along with transcription factors and histone marks, we collated genome-wide targets. Hierarchical clustering tree and heat map representation of occupancy correlation revealed three distinct ESC regulatory modules: Polycomb, Myc, and Core, as described previously (Kim et al., 2010). Jmjd2c unique targets segregated to the Polycomb module, whereas Jmjd2b unique and Jmjd2b-Jmjd2c common target genes correlated to the Core and Myc modules, respectively, which were interconnected by targets of mediators Med1 and Med12 (Figure 3H).

To determine whether genes targeted by Jmjd2b and Jmjd2c correlate with different functions as predicted by the correlation of common targets with distinct modules, we performed GO analysis. Jmjd2b-Jmjd2c common target genes were highly enriched for transcriptional regulation, DNA binding, and cell-cycle-related terms, whereas Jmjd2b and Jmjd2c unique targets related to nucleosome assembly and several development processes, respectively (Figure S3F). In addition, IPA demonstrated that Jmjd2b-Jmjd2c common target genes were closely related to DNA damage and many cancer-related pathways, such as p53, PI3K-AKT, and ESC pluripotency (Figure S3G), consistent with the Myc module (Kim et al., 2010). Meanwhile, Jmjd2c unique target genes were mainly associated with several neuronal signaling pathways (Figure S3G), compatible with association of the PRC2 module with development. Taken together, these data provide evidence that Jmjd2b and Jmjd2c act individually and combinatorially through different regulatory cassettes in mESCs.

Jmjd2b/Kdm4b and Jmjd2c/Kdm4c Interact with Key Components of Different Regulatory Modules

Nuclear factors that exhibit common targets often physically associate (Kim et al., 2010). Therefore, we examined physical interactions between Jmjd2b and Jmjd2c with core components of each regulatory module. Coimmunoprecipitation (co-IP) with Ezh2 antibody revealed an association of Jmjd2c and components of the PRC2 complex (Ezh2, Suz12, Jarid2) (Figure 3I). In contrast, other Kdm4 family members, Jmjd2a, Jmjd2b, and Jmjd2d, did not coimmunoprecipitate with Ezh2. Conversely, co-IP with Jmjd2c antibody confirmed interaction between Jmjd2c and members of the PRC2 complex, but not with key components (Nanog and Sox2) of other regulatory modules (Figure 3I). The interaction between Jmjd2c and PRC2 components is specific, as Jmjd2c does not interact detectably with the PRC1 subunit Bmi1. Jmjd2c does not interact with Jmjd2b (Figure 3I). We further examined whether stability of the PRC2 complex is affected upon depletion of Jmjd2c, and the converse. The level of Ezh2 protein was unaffected upon depletion of Jmjd2c; moreover, the level of Jmjd2c protein was unaltered upon Ezh2 depletion (Figure S3H). Finally, co-IP of Jmjd2b revealed association with Oct4, Nanog, and cMyc, but not with Ezh2 and Suz12 of the PRC2 complex (Figure 3J). These data strengthen the functional relationship between Jmjd2b and Jmjd2c with their central components of different ESC regulatory modules.

To explore molecular changes upon depletion of Jmjd2b and Jmjd2c, we examined global histone marks, including H3K9me2/me3 and H3K36me2/me3, the putative substrates of the Jmjd2b and Jmjd2c demethylases (Cloos et al., 2006; Agger et al., 2008). We did not observe significant global changes, including H3K9me2/me3 and H3K36me2/me3 (Figures S3I and S3J). To examine potential redundant function of Jmjd2b and Jmjd2c for these histone modifications, knockdown of both Jmjd2b and Jmjd2c was performed (Figure S3K). An increased level of global H3K9me3 was observed (Figure S3L). This finding implies redundant or overlapping roles among the members of the same subclass.

Figure 2. Jmjd2b/Kdm4b and Jmjd2c/Kdm4c Are Essential for mESC Identity

(A) Hierarchical clustering of gene expression profiles from Anti-GFP (control) and Jmjd2b (Jmjd2b-1 and Jmjd2b-4 shRNAs) and Jmjd2c (Jmjd2c-1 and Jmjd2c-2 shRNAs) depleted cells. The average fold change from two different shRNAs was calculated. The heat map represents the z score of expression values, whereas the red curve shows the relative expression changes of these cluster genes between undifferentiated and differentiated ESCs smoothed by a moving window of size 50.

(B) Venn diagrams representing overlapping up- or downregulated genes between Jmjd2b and Jmjd2c depleted cells.

(C and D) Gene expression analyses for ESC-specific genes and lineage-specific differentiation genes from Jmjd2b and Jmjd2c depleted cells. Gapdh and actin were used as internal controls. Data shown are averaged from three biological replicates. Data are represented as mean ± SEM; n = 3; p values were calculated using ANOVA; $p < 0.01$.

(E and F) GSEA of a differentially expressed gene set of Jmjd2b and Jmjd2c depleted cells. NES, normalized enrichment score; p, nominal p value.

See also Figure S2.

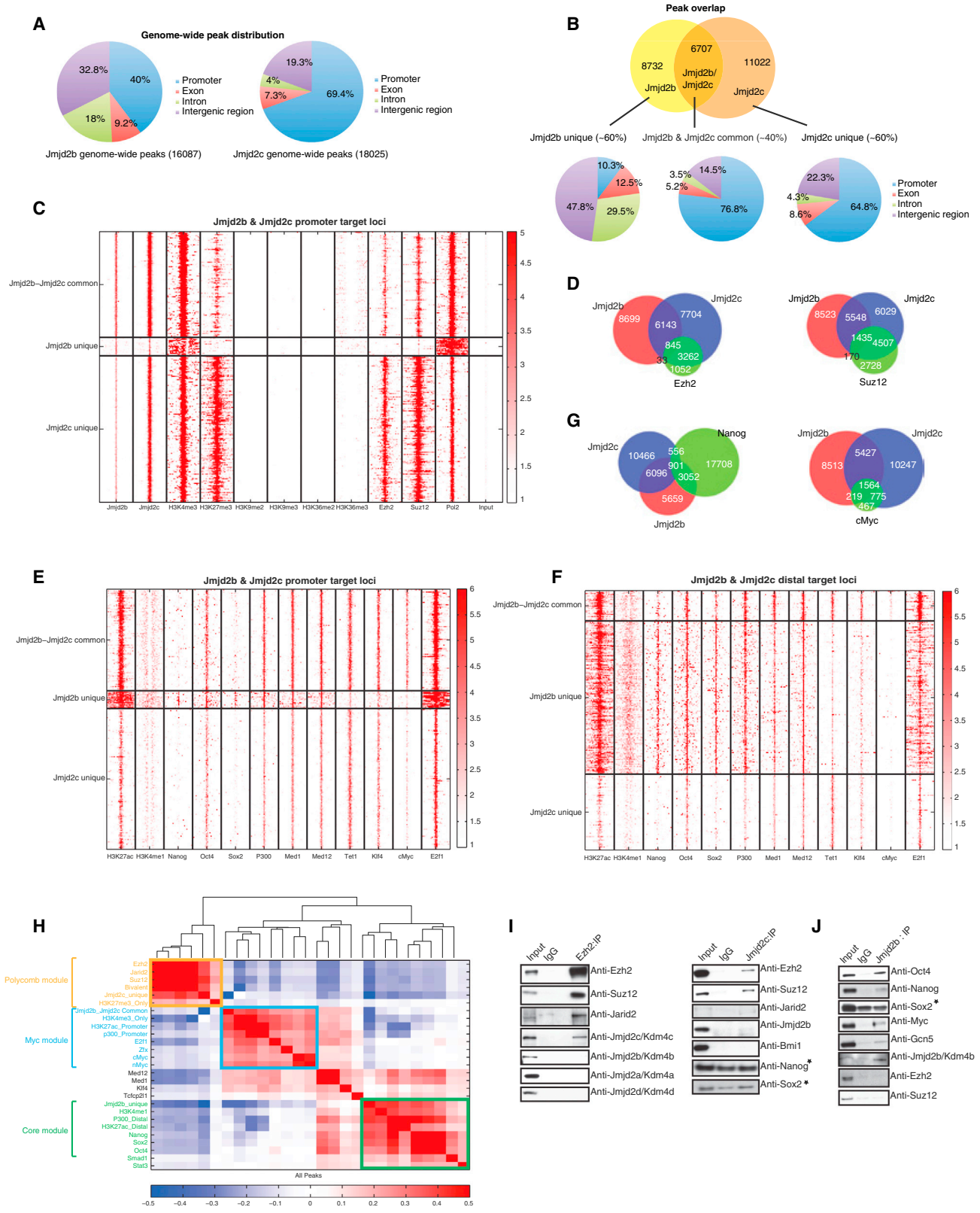

(legend on next page)

Jmjd2b/Kdm4b and Nanog Act through an Interconnected Regulatory Loop

To interrogate potential molecular mechanisms of Jmjd2b action, we generated ChIP-seq data sets of Nanog, Oct4, and cMyc, as well as histone marks H3K4me3, H3K27me3, H3K36me3, H3K9me3, and H3K27ac from both control (Anti-GFP) and Jmjd2b-depleted ESCs. We calculated the $\log_2$ ratio (M value) of ChIP-seq intensities between the two cell types using MAnorm, a quantitative comparison algorithm (Shao et al., 2012). The vast majority of Nanog binding peaks were reduced >2-fold upon Jmjd2b knockdown (corresponding to M value < -1) (Figure 4A; Table S7). As Jmjd2b unique targets predominantly occupy distal regions, we assessed H3K27ac occupancy at distal regions from control and Jmjd2b depleted cells. Global occupancy of H3K27ac was unchanged at both promoter and distal regions upon depletion of Jmjd2b (Figure 4B). Further analyses showed that global Nanog occupancy was not dependent on Jmjd2b occupancy (Figure 4C), although global Nanog occupancy was reduced significantly upon depletion of Jmjd2b, suggesting other mechanisms by which Jmjd2b regulates Nanog binding.

To investigate how Jmjd2b impinges on the Nanog regulatory pathway, we examined expression of Nanog upon Jmjd2b knockdown and observed significant reduction of Nanog, but not Oct4, expression (Figures 4D and 4E). Subsequently, we examined binding of Jmjd2b, Jmjd2c, Nanog, Oct4, mediators (Med1 and Med12), and H3K27ac specifically at the *Nanog* locus, and observed loss of Nanog binding selectively at its enhancer locus upon Jmjd2b knockdown (Figure 4F). Similarly, reduction or loss of Nanog binding was also found at regulatory regions of several of its downstream target genes, including both ESC-specific (*Klf4* and *Tbx3*) and lineage-specific genes (*Lefty1* and *Otx2*) upon knockdown of Jmjd2b (Figure 4G; Figures S4A–S4C). Next, we determined whether Nanog regulates Jmjd2b expression; surprisingly, we found that expression of Jmjd2b was also reduced upon depletion of Nanog (Figure 4H) and that occupancy of Nanog was reduced at the *Jmjd2b* locus in Jmjd2b knockdown cells (Figure 4I), suggesting that Jmjd2b and Nanog control each other through a regulatory loop. Furthermore, we compared global gene expression changes upon knockdown of Jmjd2b, Jmjd2c, Oct4, and Nanog. We observed the highest correlation of global gene expression changes between Jmjd2b and Nanog knockdown samples (Figure 4J). Genes differentially expressed upon knockdown of Nanog significantly overlapped with differentially expressed genes following Jmjd2b depletion (Figure 4K), indicating that their regulatory pathways are tightly interconnected. Further analyses revealed that the combined binding targets of Jmjd2b and Nanog highly correlated with Jmjd2b-depleted downregulated genes, whereas Nanog-only binding targets were correlated with Jmjd2b-depleted upregulated genes (Figure 4L). These findings are consistent with the prior observation that Nanog acts combinatorially in target gene activation but binds alone or with few other proteins at repressed or nonexpressed targets (Kim et al., 2008). Taken together, our data argue that Jmjd2b and Nanog act through highly interconnected regulatory pathways.

To test this further, we performed rescue experiments with full-length Jmjd2b, the catalytic domain (JmjC) of Jmjd2b (1–333 aa), a catalytic mutant (HTE>ATA) of Jmjd2b, and full-length Nanog in *Jmjd2b*-deficient ESCs (Figures S1F, S4L and S4M). Full-length Jmjd2b fully rescued Nanog expression, and vice versa, in *Jmjd2b*-deficient ESCs, whereas the catalytic domain (JmjC)-containing Jmjd2b (1–333 aa) and the catalytic mutant (HTE>ATA) of Jmjd2b only partially rescued Nanog expression (Figures S4L and S4M), which is correlated with the restored ESC growth phenotype and SSEA-1 expression (Figure S1F).

Our findings fail to replicate a prior report that Jmjd2c binds at the *Nanog* promoter and regulates Nanog expression through H3K9me3 levels (Loh et al., 2007). We observed Jmjd2b occupancy at the *Nanog* locus, but did not detect a change in H3K9me3 at this locus upon depletion of Jmjd2b (Figure S4D). Moreover, we observed significant reduction of Nanog expression and occupancy at target genes (*Nanog*, *Klf4*, *Otx2*) upon depletion of Jmjd2b but not upon depletion of Jmjd2c (Figure S4E), suggesting Jmjd2b-Nanog interconnected regulation.

Jmjd2c/Kdm4c Assists PRC2 in Repression in mESCs

Jmjd2c associates with the PRC2 complex, and targets of Jmjd2c in chromatin correlate with the PRC2 regulatory module. To gain insight into these relationships, we performed ChIP-seq of Oct4, Nanog, Ezh2, cMyc, H3K4me3, H3K27me3, H3K36me3, and H3K9me3 in both control (Anti-GFP) and

Figure 3. Genome-wide Mapping of Jmjd2b/Kdm4b and Jmjd2c/Kdm4c in mESCs by ChIP-Seq

(A) Pie charts showing genome-wide peak distribution of Jmjd2b and Jmjd2c.

(B) Venn diagram showing the number of Jmjd2b and Jmjd2c overlapped and unique peaks. Pie charts represent the distribution of Jmjd2b unique, Jmjd2c unique, and Jmjd2b-Jmjd2c common peaks.

(C and E) Heat maps showing the ChIP intensities of selected histone marks, TFs, and chromatin regulators including components of PRC2 and RNA Pol II at the ±5 kb regions around the peak summit of Jmjd2b unique, Jmjd2c unique, and Jmjd2b-Jmjd2c common promoter target loci.

(D and G) Venn diagram showing the peak overlaps between Jmjd2b, Jmjd2c, and the other factors Ezh2, Suz12, Nanog, and cMyc.

(F) Heat map showing the ChIP intensities of histone marks, TFs, and chromatin regulators at the ±5 kb regions around the peak summit of Jmjd2b unique, Jmjd2c unique, and Jmjd2b-Jmjd2c common target loci at distal regions.

(H) Correlation map of binding loci showing the degree of co-occupancy between selected histone modifications, TFs, chromatin regulators, and three peak sets defined by the combination of Jmjd2b and Jmjd2c as described in (B). Here, the color scale represents the Pearson correlation coefficient, and the clustering tree is derived from hierarchical clustering.

(I) Coimmunoprecipitation using antibodies against Ezh2, Jmjd2c, and IgG. Endogenous Ezh2 and Jmjd2c were immunoprecipitated from nuclear extracts of mESCs, and their interacting partners were analyzed by western blot using antibodies as shown on the right. Asterisks indicate unspecific interactions.

(J) Jmjd2b antibody was used to immunoprecipitate endogenous Jmjd2b from nuclear extracts of mESCs, and its interacting partners were analyzed by western blot using antibodies. The asterisk indicates unspecific interactions.

See also Figure S3.

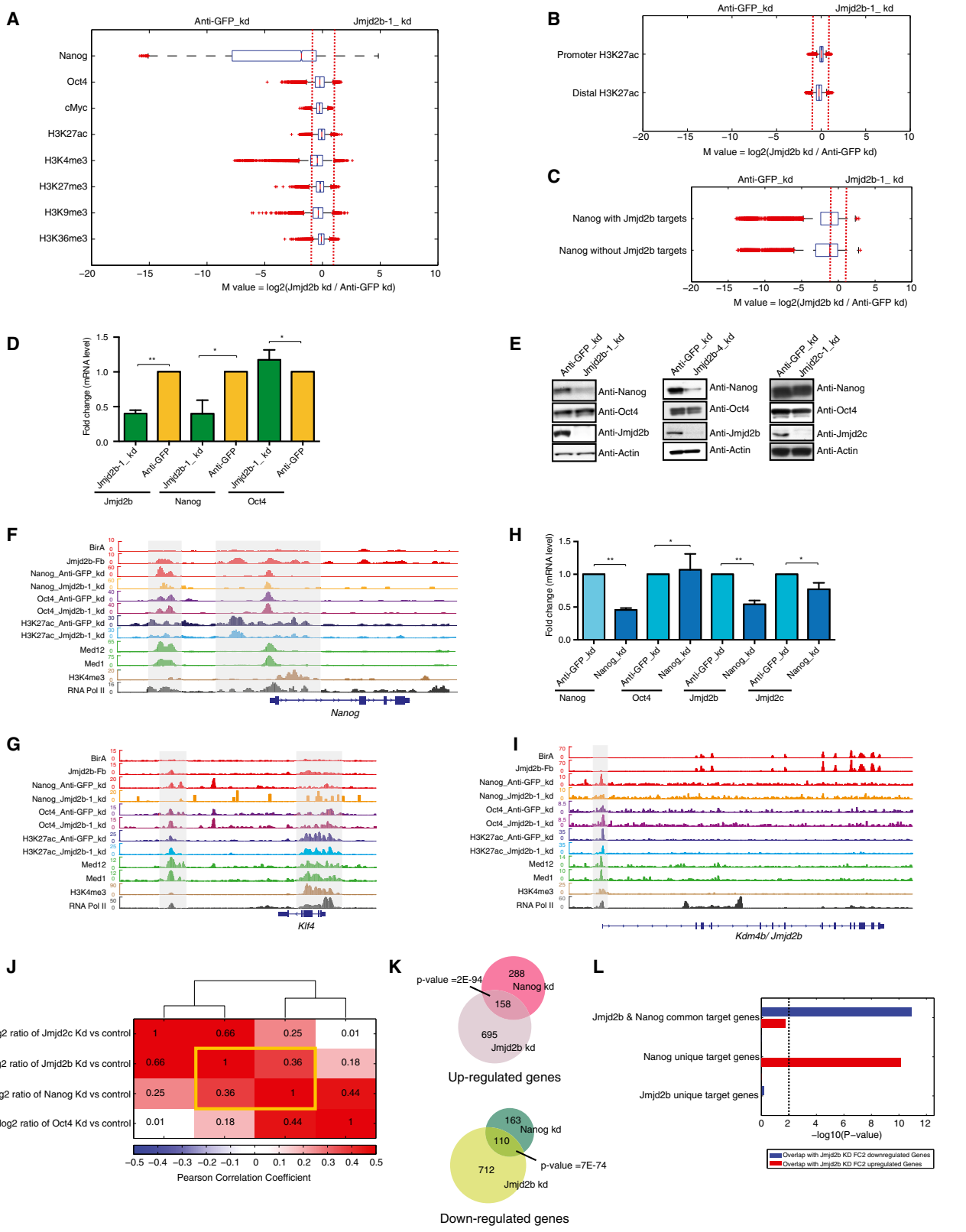

(legend on next page)

Jmjd2c knockdown mESCs. Quantitative comparison indicated that none of these factors demonstrated a significant global change of binding intensity (Figure 5A; Table S7), suggesting that the predominant effect of Jmjd2c depletion is restricted to a subset of genes.

Genes that displayed increased expression upon Jmjd2c knockdown were composed principally of developmentally regulated genes (Figures S2D and S2E). Because this class is highly enriched in bivalent marks (and the presence of Ezh2) in ESCs, we compared the binding of Ezh2/H3K27me3 and Jmjd2c at the promoter region of these genes. We observed highly significant co-occupancy of Jmjd2c and Ezh2 at these Jmjd2c-depleted upregulated genes (Figure 5B). Yet neither Jmjd2c nor Ezh2 alone significantly occupies these upregulated genes, suggesting that Jmjd2c and Ezh2 act combinatorially in gene repression and that Jmjd2c exerts a direct gene regulatory influence through occupancy of these promoters (Figure 5B). Moreover, Jmjd2c knockdown did not significantly alter occupancy of Ezh2/H3K27me3 at Jmjd2c-depleted upregulated genes (Figure 5C; Figure S5A), indicating that Ezh2 alone is insufficient to repress these upregulated genes and requires Jmjd2c for full repression. Further study of several developmental genes, *Pitx2*, *Fgf5*, *Wnt3*, *T*, and *Olig3* that were strongly upregulated in Jmjd2c knockdown cells, showed that indeed these gene loci are occupied by both Jmjd2c and Ezh2. However, the binding of Ezh2 and the presence of H3K27me3 were largely "invariant" at these loci upon depletion of Jmjd2c (Figures 5D and 5F; Figures S5B and S5C). Thus, although recruitment of PRC2/Ezh2 and H3K27me3 deposition are independent of Jmjd2c, full repression associated with PRC2 at these targets requires Jmjd2c.

Jmjd2c/Kdm4c and PRC2 Block Transcription at PRC2 Target Genes

Because the H3K27me3 mark is largely unchanged at upregulated genes upon Jmjd2c depletion (Figures 5C–5F; Figure S5A), we speculated that Jmjd2c might affect other aspects of PRC2-mediated repression. Recent studies indicate that bivalent genes bound by PRC2 exhibit RNA Pol II pausing at proximal promoters with reduction of productive transcriptional elongation (Min et al., 2011), thereby providing another mechanism of repression. Through co-IP, we observed that both Ezh2 and Jmjd2c interact with pausing factors (NelfA and Spt5), as well as with components of the core transcription machinery involved in initiation and elongation, including unphosphorylated RNA Pol II (RNAP) (initiation), RNA Pol II Ser-5p (RNAP-S5p) (initiation), RNA Pol II Ser-2p (RNAP-S2p) (elongation), Cdk9 (initiation), Ctr9 (component of Paf1c elongation complex), and cMyc (initiation; involved in pause release) (Peterlin and Price, 2006; Rahl et al., 2010; Nechaev and Adelman, 2011) (Figure S6A). Furthermore, full-length Jmjd2c, as well as its catalytic domain (1–333 aa), interacted with Ezh2, RNAP, and Cdk9 (Figure S6B).

To gain further insights into the mechanistic role of Jmjd2c and Ezh2 in RNA Pol II pausing, we examined three sets of genes defined by promoter occupancy of Jmjd2b, Jmjd2c, H3K4me3, and H3K27me3: Jmjd2b-Jmjd2c common active genes (H3K4me3-only), Jmjd2c unique active genes (H3K4me3-only), and all H3K27me3 repressed genes (including both bivalent and H3K27me3-only genes, most of which are PRC2 target genes and overlap with Jmjd2c target genes) (Figure 6A; Figure S3D). Jmjd2b-Jmjd2c common active genes showed strong binding of transcription initiation factors, including RNAP, RNAP-S5p, NelfA, Spt5, and cMyc at the transcription start site (TSS), as well as strong occupancy of factors associated with elongation, including RNAP-S2p, Ctr9, Spt5, H3K36me3, and H3K79me2 at gene bodies (Figure 6A). Binding of these transcription initiation and elongation factors at Jmjd2c unique active genes was reduced compared to Jmjd2b-Jmjd2c common active genes. In addition, repressed genes bound by Jmjd2c and PRC2 (H3K27me3) showed dramatic loss of binding of these factors at the TSS and gene bodies (Figure 6A), indicating that they are indeed poised/repressed in mESCs. Furthermore, comparing the expression levels among these three sets of genes confirmed that they exhibit significantly different levels of expression, which are themselves correlated with occupancy of transcription initiation and elongation factors (Figure 6B). Specifically, we observed that combined PRC2/Jmjd2c target genes are occupied by RNAP, RNAP-S5p, NelfA, and

Figure 4. Jmjd2b/Kdm4b and Nanog Act through an Interconnected Regulatory Loop

(A) Box plots of the $\log_2$ fold changes of binding intensities between Anti-GFP (control) and Jmjd2b knockdown (KD) ESCs for Nanog, Oct4, cMyc, H3K27ac, H3K4me3, H3K27me3, H3K36me3, and H3K9me3. Red crosses correspond to outliers.

(B) Box plot of the $\log_2$ fold changes of H3K27ac marks at its promoter and distal targets from Anti-GFP (control) and Jmjd2b KD cells.

(C) Box plot of the $\log_2$ fold changes of Nanog binding intensities with or without Jmjd2b occupancy in Anti-GFP (control) and Jmjd2b KD cells.

(D) mRNA expression levels of Jmjd2b, Nanog, and Oct4 from Anti-GFP (control) and Jmjd2b KD cells. Transcript levels were normalized using Gapdh. Data are represented as mean ± SEM; n = 3; p values were calculated using t test; $^{**}p < 0.001$, $^{*}p < 0.01$.

(E) Western blot analyses of Nanog and Oct4 from Jmjd2b (using two individual shRNAs) and Jmjd2c and Anti-GFP (control) depleted cells.

(F and G) Genomic tracks of ChIP intensities of factor and histone mark binding at *Nanog* and *Klf4* loci.

(H) mRNA expression levels of Jmjd2b, Jmjd2c, Oct4, and Nanog from Nanog KD and Anti-GFP KD (control) cells. Transcript levels were normalized using Gapdh. Data are represented as mean ± SEM; n = 3; p values were calculated using t test; $^{**}p < 0.001$, $^{*}p < 0.01$.

(I) Genomic tracks of ChIP intensities of factor and histone mark binding at the *Kdm4b*/*Jmjd2b* locus. Jmjd2b shows no enrichment of its binding at its own locus.

(J) Clustering patterns of global gene expression changes by $\log_2$ ratio in Jmjd2b, Jmjd2c, Nanog, and Oct4 depleted cells relative to their corresponding controls. Colors and numbers represent the Pearson correlation coefficient.

(K) Venn diagram of overlapped up- or downregulated genes in Jmjd2b and Nanog knockdown cells.

(L) p values represent enrichment of overlap between up- or downregulated genes in Jmjd2b knockdown cells compared to Anti-GFP (control) knockdown cells and target genes occupied by either Jmjd2b or Nanog or both in mESCs (see Supplemental Experimental Procedures for the definition of Jmjd2b and Nanog ChIP target genes). The height of the bars represents a −log10-transformed p value, derived from right-tailed Fisher's exact test, and the dotted line corresponds to a p value of 0.01, above which overlap will be considered as significantly enriched.

See also Figure S4.

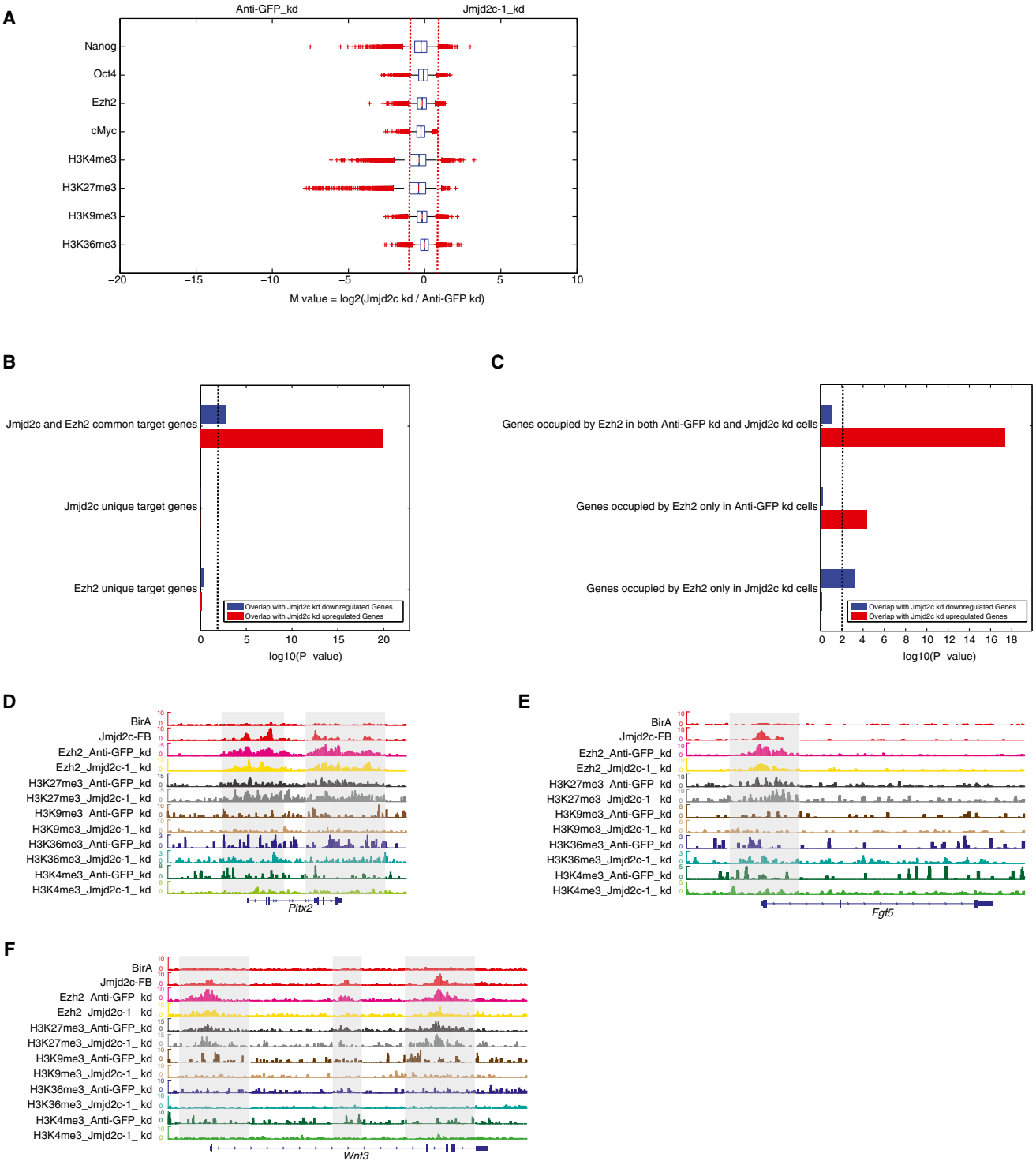

Figure 5. Jmjd2c/Kdm4c Assists PRC2 in Repression in mESCs

(A) Box plots of the $\log_2$ fold change of binding intensities between Anti-GFP (control) and Jmjd2c depleted cells for Nanog, Oct4, Ezh2, cMyc, H3K4me3, H3K27me3, H3K36me3, and H3K9me3. Red crosses correspond to outliers.

(B) p values represent enrichment of overlap between up- or downregulated genes from Jmjd2c knockdown cells compared to Anti-GFP (control) knockdown cells and target genes occupied by either Jmjd2c or Ezh2 or both in mESCs at promoters. The height of the bars represents −log10-transformed p value derived from right-tailed Fisher's exact test, and the dotted line corresponds to a p value of 0.01.

(legend continued on next page)

Spt5 at the promoter regions but not with elongation factors (RNAP-S2p, Ctr9, H3K36me3, and H3K79me2) at gene bodies, suggesting that these poised/repressed genes are probably paused with RNA Pol II (Figure 6A) (Nechaev and Adelman, 2011). We observed that cMyc occupancy directly correlated with transcription of two sets of active genes but not with PRC2 target genes (Figure 6A), consistent with a role for cMyc in active transcription through RNA Pol II pause release at actively transcribed genes in mESCs (Rahl et al., 2010). These data point to a role for Jmjd2c in transcriptional repression, most likely through blocking of RNA Pol II recruitment and/or pausing of RNA Pol II at Jmjd2c-occupied PRC2 target genes.

Next, we examined occupancy of selected factors and histone marks involved in transcription initiation and elongation in Jmjd2c and control (Anti-GFP) knockdown cells. Global occupancy of these factors and histone marks did not differ significantly between these cells (Figure 5A; Figure S6C; Table S7). We then used a quantitative comparison method to discover factors whose binding is altered significantly at Jmjd2c-depleted up- and downregulated genes (see Supplemental Experimental Procedures for detailed methods). Jmjd2c depleted upregulated genes reveal significantly higher binding of RNAP, RNAP-S5p, RNAP-S2p, Ctr9, and H3K36me3 mark (a mark associated with transcription elongation), whereas Jmjd2c-depleted downregulated genes showed reduced occupancy of these factors and histone marks (Figure 6C; Figure S6D). Moreover, we observed increased and decreased occupancy of transcription initiation and elongation factors at specific upregulated and downregulated gene loci, respectively, upon Jmjd2c depletion (Figures 6D–6I; Figures S6E–S6H), indicating correlation between occupancy of the transcription machinery and gene expression. We demonstrate that Jmjd2c and Ezh2 co-occupy significantly at Jmjd2c-depleted upregulated genes compared to downregulated genes (Figure 5B) and that these upregulated genes display increased binding of transcription machinery factors and histone marks upon depletion of Jmjd2c, suggesting that Jmjd2c directly regulates these upregulated genes. On the other hand, no correlation was observed between Jmjd2c occupancy and Jmjd2c-depleted downregulated genes (Figure 5B), indicative of indirect regulation of these genes through Jmjd2c. Taken together, these data indicate that Jmjd2c is required in ESCs for full repression by PRC2 at poised/repressed developmental genes.

DISCUSSION

Jmjd2b/Kdm4b and Jmjd2c/Kdm4c Belong to Distinct Regulatory Modules in mESCs

Depletion of either Jmjd2b or Jmjd2c leads to ostensibly similar differentiation phenotypes and comparable overall global gene expression patterns in ESCs (Figures 1B and 2; Figure S1B). However, global chromatin occupancy studies of Jmjd2b and Jmjd2c demonstrate that each occupies numerous unique and common targets and correlates with functionally distinct regulatory modules. Jmjd2b unique, Jmjd2b-Jmjd2c common, and Jmjd2c unique targets partition to the Core, Myc, and PRC regulatory modules of the overall ESC network, respectively (Figure 3H). Thus, these closely related HDMs subserve specialized targets, in part relating to their combinatorial partitioning. Metagene analyses provide further support that occupancy of Jmjd2b and Jmjd2c unique and common targets is correlated with the pattern of gene expression in mESCs (Figure S3C). Protein-protein interaction studies corroborate that Jmjd2b and Jmjd2c physically interact with distinct regulators, specifically Jmjd2b with factors of the Core pluripotency network and Jmjd2c with components of the PRC2 complex (Figures 3I and 3J). Therefore, we speculate that combinatorial binding patterns of HDMs across the genome will be critical for understanding regulatory programs in cell-type-specific transcriptional regulation.

Jmjd2b/Kdm4b, Jmjd2c/Kdm4c, and Histone Modifications

Combinations of histone modifications play a crucial role in gene regulation (Zhou et al., 2011). Jmjd2b and Jmjd2c are classified as H3K9me2/3 and H3K36me2/3 HDMs (Agger et al., 2008; Cloos et al., 2006). As H3K36me2/me3 and H3K9me2/3 are indicative of divergent transcriptional outcomes, it is possible that Jmjd2b and Jmjd2c function differently in a cell-type-specific and context-dependent manner. A relatively low level of H3K9me3 correlates with the highly active and open ESC and iPSC genome (Meshorer and Misteli, 2006; Soufi et al., 2012). Recent studies also demonstrate that depletion of all H3K9 demethylases, including Jmjd2b and Jmjd2c, significantly inhibits reprogramming of pre-iPSCs to iPSCs. Conversely, depletion of the H3K9 methyltransferase Setdb1 leads to highly efficient reprogramming, indicating that removal of H3K9me3 is essential for establishment of the ESC/iPSC state (Chen et al., 2013). In this study, we did not observe significant changes in "global" histone levels or occupancy, including H3K9me2/3 and H3K36me2/3 marks, upon depletion of either Jmjd2b or Jmjd2c (Figures 4A and 5A; Figures S3I and S3J). However, double knockdown of Jmjd2b and Jmjd2c led to an increased level of global H3K9me3 (Figures S3K and S3L), suggesting a redundant function in ESCs. We also monitored the effects of Jmjd2b and Jmjd2c depletion on histone marks (H3K4me3, H3K27me3, H3K9me3, and H3K36me3) at several "individual" loci. For Jmjd2b-Jmjd2c common active genes, we observed reduction of H3K4me3 and H3K36me3 occupancy at several active gene loci, such as *Klf4*, *Tbx3*, and *Esrrb*, upon depletion of either Jmjd2b or Jmjd2c (Figure 7; Figures S4F–S4K and S7A–S7C). In the context of Jmjd2b-Nanog interconnected regulation, we did not observe any significant change of H3K9me3 at the *Nanog* locus and its downstream target genes upon depletion of Jmjd2b. However, we observed occupancy changes at several

(C) p values represent enrichment of overlap between up- or downregulated genes from Jmjd2c knockdown cells compared to Anti-GFP (control) knockdown cells and the promoter target genes of Ezh2 in these two cell types. The p value represents the same as in (B).
(D–F) Genomic tracks of ChIP-seq intensities of Jmjd2c, Ezh2, and histone marks in both Anti-GFP (control) and Jmjd2c KD cells at selected upregulated gene loci upon Jmjd2c depletion (*Pitx2*, *Fgf5*, and *Wnt3*).
See also Figure S5.

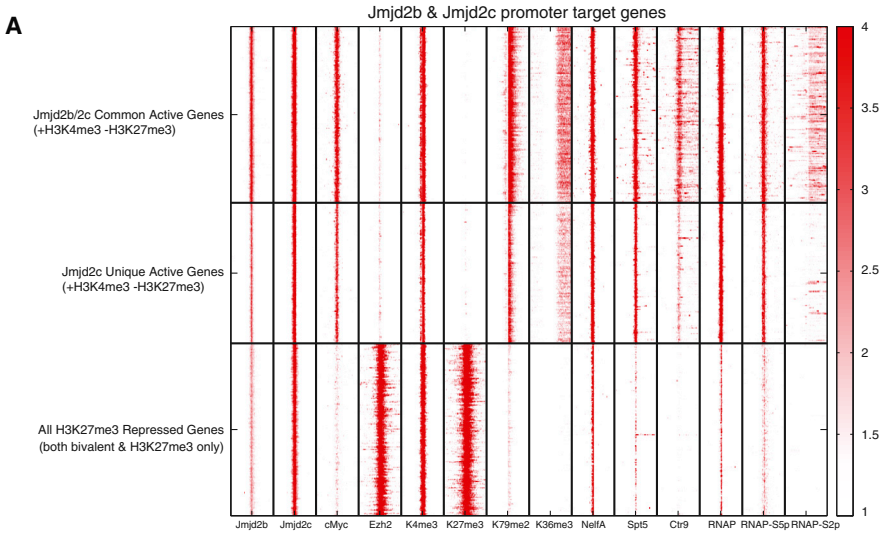

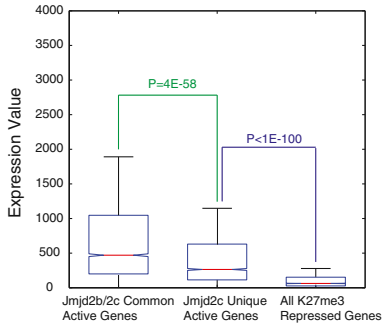

C

Significance of differential binding of factors and histone marks at Jmjd2c up and down regulated genes

Name	Up-regulated genes (p-value)	Down-regulated genes (p-value)
RNA Pol II	1.7E −06	1.0E −06
RNA Pol II Ser5p	0.001	4.4E −09
RNA Pol II Ser2p	0.005	0.0017
Ctr9	0.0002	NS
Spt5	NS	3E−18
H3K36me3	3.7E-05	4.5E −20
Ezh2	NS	0.00017
H3K27me3	NS	NS
H3K4me3	NS	NS
cMyc	NS	NS
H3K9me3	NS	NS

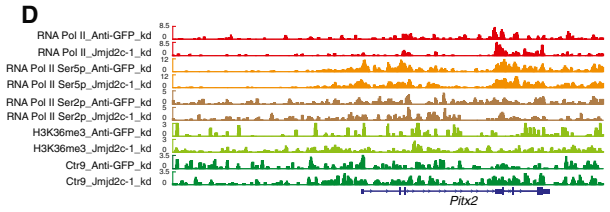

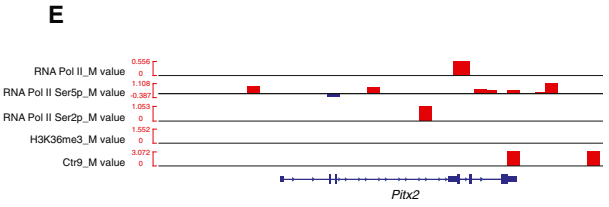

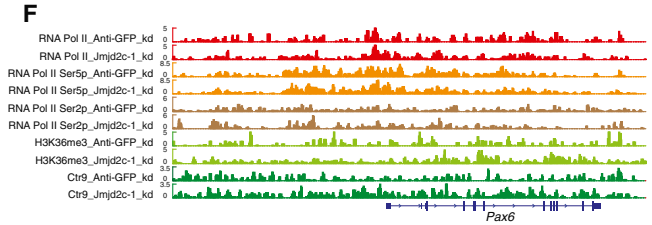

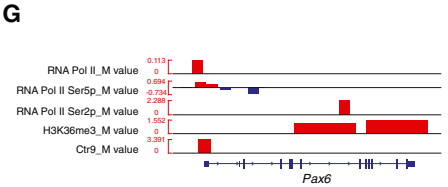

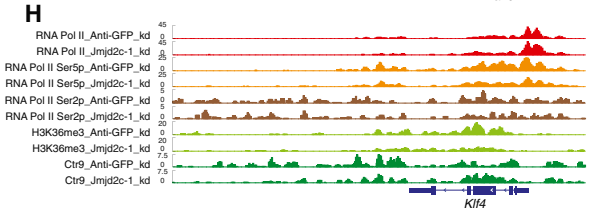

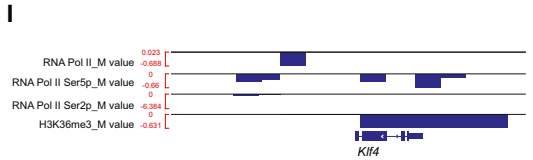

(legend on next page)

discrete loci for H3K4me3 (e.g., *Nanog*, *Klf4*, *Tbx3*, and *Esrrb* promoters) and H3K36me3 (e.g., *Klf4*, *Tbx3*, and *Otx2* gene bodies) (Figure 7; Figures S4F–S4K). Interestingly, we found that some of the Jmjd2b-Jmjd2c common active genes are the downstream targets of Nanog, suggesting a fraction of common targets is regulated through the Jmjd2b-Nanog regulatory loop (Figures 4G and 7; Figures S4A–S4C and S7A–S7C). On the other hand, with respect to the role of Jmjd2c in PRC2-mediated repression, we observed that the upregulated genes upon Jmjd2c depletion are significantly co-occupied by Jmjd2c and Ezh2, and that Jmjd2c assists PRC2 in full repression at these poised/repressed genes (e.g., *Fgf5*, *Pitx2*, *Pax6*) through transcription repression (Figure 5B). Moreover, these upregulated genes showed significantly increased binding of the transcriptional machinery (RNAP, RNAP-S5p, RNAP-S2p, Ctr9) and histone marks, especially H3K36me3 (an elongation mark), but not other histone marks upon depletion of Jmjd2c (Figures 6C–6I and 7; Figures S6D–S6H), indicative of a link between Jmjd2c-PRC2 and transcription elongation. This supports a previous observation in which Polycomb-like-PRC2 recognizes H3K36me3 and silences active chromatin regions for maintenance of ESC pluripotency (Cai et al., 2013).

Our study reveals unexpected outcomes of the histone demethylase function of Jmjd2b and Jmjd2c and its substrate specificity. However, rescue studies demonstrate that catalytic activity of Jmjd2b and Jmjd2c is indeed required for self-renewal of ESCs. Moreover, our findings indicate a complex interplay between various histone modifications and/or that Jmjd2b and Jmjd2c may have additional roles beyond histone targets. Recent studies have indicated that Jmjd2b is an integral part of the MLL2 complex that deposits the H3K4me3 mark, and H3K9me3 is a prerequisite of H3K4me3 deposition for ERα-activated gene transcription (Shi et al., 2011), suggesting crosstalk between histone modifications.

Jmjd2b/Kdm4b and Jmjd2c/Kdm4c Act through Distinct and Combinatorial Pathways in mESCs

As a core pluripotency factor, Nanog functions together with other Core transcription factors (such as Oct4 and Sox2) to positively regulate their expression through autoregulatory loops, as well as occupy and activate ESC-specific genes and repress lineage-specific genes to maintain the ESC state (Young, 2011). We demonstrate that Jmjd2b is involved in the regulation of Nanog expression and occupancy of its downstream target genes. Moreover, Nanog regulates Jmjd2b expression that is important for maintenance of Nanog expression through a feedback loop (Figures 4A–4I and 7).

In contrast, Jmjd2c physically interacts with components of the PRC2 repressive complex, and its targets correlate with the PRC regulatory module (Figure 3). Furthermore, PRC2 requires Jmjd2c for full repressive function (Figure 5). Although the molecular details of PRC2-mediated gene repression remain incomplete, previous studies implicate several mechanisms in the control of transcriptional output including the recruitment block of RNA Pol II, as well as promoter-proximal pausing of RNA Pol II at PRC2 target genes (Boyer et al., 2006; Lee et al., 2006; Min et al., 2011). Our data suggest that Jmjd2c may influence PRC2 activities for both RNA Pol II recruitment and pausing at PRC2/Jmjd2c targets (Figures 6A–6C; Figures S6A–S6D). High co-occupancy of Jmjd2c-Ezh2 at Jmjd2c-depleted upregulated genes (Figure 5B) and increased distribution of RNAP, RNAP-S5p, RNAP-S2p, Ctr9, and H3K36me3 at these Jmjd2c/PRC2-targeted upregulated genes in Jmjd2c-depleted cells (Figures 6C–6I; Figures S6D–S6H) argue persuasively for the role of Jmjd2c in transcriptional repression. Therefore, Jmjd2c is required for the full repressive function of PRC2 at PRC2/Jmjd2c common target genes in ESCs.

Global Jmjd2b and Jmjd2c targets are differentially distributed. However, Jmjd2b and Jmjd2c share ~40% common targets (Figure 3B). These common targets are associated with active genes and belong to Myc modules (Figure 3). Jmjd2b and Jmjd2c do not physically interact with each other, but both Jmjd2b and Jmjd2c can physically interact with cMyc (Figure 3J; Figure S6A). Nevertheless, occupancy of cMyc is not significantly changed globally or locally upon depletion of either Jmjd2b or Jmjd2c (Figures 4A and 5A; Figure S7). Interestingly, we found that some of the Jmjd2b-Jmjd2c common active genes (*Klf4*, *Tbx3*, and *Esrrb*) are downstream targets of Nanog and its occupancy was reduced at these loci upon depletion of Jmjd2b, suggesting a fraction of common targets is regulated through the Jmjd2b-Nanog regulatory loop. We observed reduction of H3K4me3 and H3K36me3 at these common target genes upon depletion of either Jmjd2b or Jmjd2c (Figures S4 and S7) suggesting, indeed, that Jmjd2b and Jmjd2c combinatorially regulate these active gene loci.

We present a model in Figure 7 that summarizes our findings regarding how Jmjd2b and Jmjd2c exert both distinct and combinatorial functions in ESC identity (Figure 7). Our study suggests that exploration of combinatorial roles of HDMs with other chromatin regulators, transcription factors, and histone marks will elucidate multilayered regulatory networks in ESC biology.

Figure 6. Jmjd2c/Kdm4c and PRC2 Block Transcription at PRC2 Target Genes

(A) Heat map showing the ChIP-seq densities of selected factors, histone marks, and a different modified form of RNA Pol II (RNAP, RNAP-S5p, and RNAP-S2p) at the ±5 kb regions around the TSS of promoters of Jmjd2b-Jmjd2c common active genes, Jmjd2c unique active genes, and all H3K27me3 target genes.

(B) Box plot of gene expression values of Jmjd2b-Jmjd2c common active genes, Jmjd2c unique active genes, and all H3K27me3 target genes.

(C) Significance of binding changes of profiled factors at differentially expressed genes in Jmjd2c KD cells relative to Anti-GFP (control) KD cells. p values were calculated by using Kolmogorov-Smirnov test to compare the global distribution of $\log_2$ fold changes of ChIP intensities (M values inferred by MAnorm) of each factor at its peak loci associated with up- or downregulated genes relative to those with nondifferentially expressed genes as control. Significant p values (<0.01) are marked in red or green; otherwise they are labeled as nonsignificant (NS).

(D, F, and H) Genomic tracks represent ChIP intensities of transcription initiation and elongation factor binding in Jmjd2c KD and Anti-GFP (control) KD cells at Jmjd2c depleted upregulated (*Pitx2*, *Pax6*) and downregulated (*Klf4*) gene loci.

(E, G, and I) Genomic tracks represent the $\log_2$ fold change of binding intensities at each peak locus between selected pairs of ChIP-seq data sets shown in (D), (F), and (H), which is referred by M values derived by the MAnorm model. For further description, please see the figure legends of Figures S6F and S6H.

See also Figure S6.

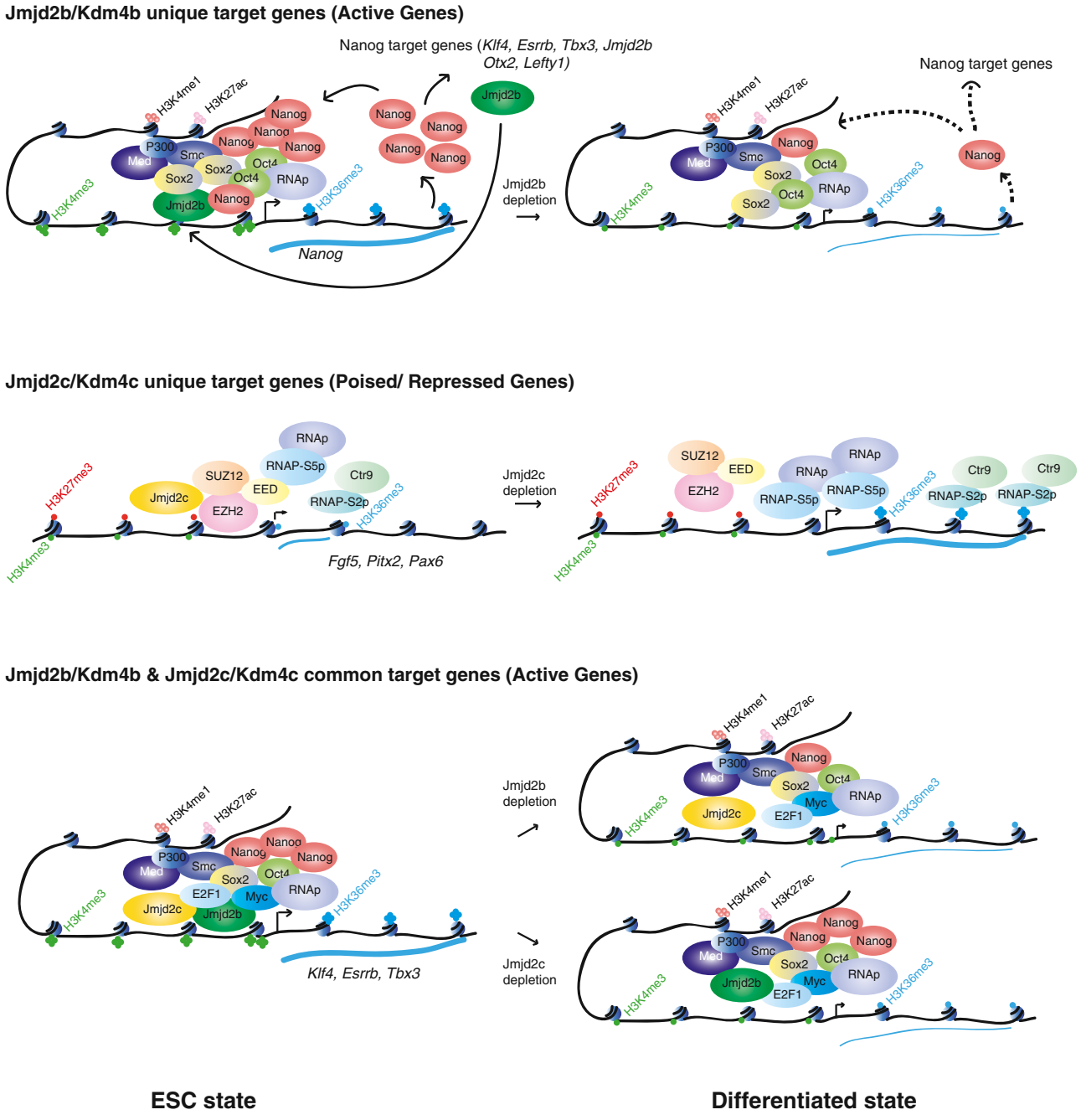

Figure 7. The Working Model of Jmjd2b/Kdm4b and Jmjd2c/Kdm4c in mESCs

Jmjd2b is generally associated with active genes, whereas Jmjd2c is associated with poised/repressive genes. However, we found that most of the active genes are occupied by both Jmjd2b and Jmjd2c. We propose a model in which Jmjd2b and Jmjd2c work distinctly and combinatorially. Blue thick and thin lines correspond to higher and lower levels of transcription, respectively. The black dotted line represents lower binding of Nanog to its target genes upon depletion of Jmjd2b.

See also Figure S7.

EXPERIMENTAL PROCEDURES

ESC Lines and Culture

Mouse ESC lines were maintained in ES medium as documented in Supplemental Experimental Procedures.

Lentiviral Production and RNAi Screen

Individual shRNA constructs were used for lentiviral production. We used five different shRNA lentiviral constructs to knock down each of 20 histone demethylases in mESCs. mESCs were seeded in 48-well plates and infected with individual shRNA lentiviruses, and the screen was scored in terms of alterations

of ESC colony morphology. A detailed protocol of lentiviral production and infection of mESCs is available in Supplemental Experimental Procedures.

Gene Expression Analysis

mRNA profiling of knocked down samples was performed using Affymetrix mouse genome 430 2.0 arrays. See Supplemental Experimental Procedures.

ChIP

Bio-ChIP and native antibody ChIP were performed as described elsewhere (Kim et al., 2008, 2009). Detailed procedures and lists of antibodies are available in Supplemental Experimental Procedures.

ChIP Sequencing and Library Generation

Purified ChIP DNA was used to prepare Illumina multiplexed sequencing libraries. A New England BioLabs Next Generation Sequencing kit was used to prepare the libraries.

ChIP-Seq Data Analysis

Peaks were called using MACS, a peak-finding algorithm to identify regions of ChIP-seq enrichment over background (Zhang et al., 2008). Detailed analyses are available in Supplemental Experimental Procedures.

Coimmunoprecipitation

Nuclear extracts were prepared from J1 mouse ESCs (Kim et al., 2010) and immunoprecipitated using specific antibodies.

ACCESSION NUMBERS

The cDNA microarray and ChIP-seq data have been deposited in the Gene Expression Omnibus (http://www.ncbi.nlm.nih.gov/geo) under accession number GSE43231.

SUPPLEMENTAL INFORMATION

Supplemental Information includes Supplemental Experimental Procedures, seven figures, and seven tables and can be found with this article online at http://dx.doi.org/10.1016/j.molcel.2013.11.011.

ACKNOWLEDGMENTS

We thank Dan Bauer, Jian Xu for critical reading of the manuscript, and David Hendrix for discussions. We also thank Marc Kerenyi for reagents. We thank F. Abderazzaq and R. Rubio at the Center for Computational Biology sequencing facility at the Dana-Farber Cancer Institute for Illumina HiSeq 2000 sequencing. This work was supported by funding from NIH grant HLBI U01HL100001. S.H.O. is an Investigator of the Howard Hughes Medical Institute.

Received: May 10, 2013
Revised: September 16, 2013
Accepted: November 13, 2013
Published: December 19, 2013

REFERENCES

Agger, K., Christensen, J., Cloos, P.A., and Helin, K. (2008). The emerging functions of histone demethylases. Curr. Opin. Genet. Dev. *18*, 159–168.

Boyer, L.A., Plath, K., Zeitlinger, J., Brambrink, T., Medeiros, L.A., Lee, T.I., Levine, S.S., Wernig, M., Tajonar, A., Ray, M.K., et al. (2006). Polycomb complexes repress developmental regulators in murine embryonic stem cells. Nature *441*, 349–353.

Cai, L., Rothbart, S.B., Lu, R., Xu, B., Chen, W.-Y., Tripathy, A., Rockowitz, S., Zheng, D., Patel, D.J., Allis, C.D., et al. (2013). An H3K36 methylation-engaging Tudor motif of polycomb-like proteins mediates PRC2 complex targeting. Mol. Cell *49*, 571–582.

Chen, X., Xu, H., Yuan, P., Fang, F., Huss, M., Vega, V.B., Wong, E., Orlov, Y.L., Zhang, W., Jiang, J., et al. (2008). Integration of external signaling pathways with the core transcriptional network in embryonic stem cells. Cell *133*, 1106–1117.

Chen, J., Liu, H., Liu, J., Qi, J., Wei, B., Yang, J., Liang, H., Chen, Y., Chen, J., Wu, Y., et al. (2013). H3K9 methylation is a barrier during somatic cell reprogramming into iPSCs. Nat. Genet. *45*, 34–42.

Cherry, A.B.C., and Daley, G.Q. (2012). Reprogramming cellular identity for regenerative medicine. Cell *148*, 1110–1122.

Cloos, P.A.C., Christensen, J., Agger, K., Maiolica, A., Rappsilber, J., Antal, T., Hansen, K.H., and Helin, K. (2006). The putative oncogene GASC1 demethylates tri- and dimethylated lysine 9 on histone H3. Nature *442*, 307–311.

Fazzio, T.G., Huff, J.T., and Panning, B. (2008). An RNAi screen of chromatin proteins identifies Tip60-p400 as a regulator of embryonic stem cell identity. Cell *134*, 162–174.

Hu, G., Kim, J., Xu, Q., Leng, Y., Orkin, S.H., and Elledge, S.J. (2009). A genome-wide RNAi screen identifies a new transcriptional module required for self-renewal. Genes Dev. *23*, 837–848.

Kagey, M.H., Newman, J.J., Bilodeau, S., Zhan, Y., Orlando, D.A., van Berkum, N.L., Ebmeier, C.C., Goossens, J., Rahl, P.B., Levine, S.S., et al. (2010). Mediator and cohesin connect gene expression and chromatin architecture. Nature *467*, 430–435.

Kim, J., Chu, J., Shen, X., Wang, J., and Orkin, S.H. (2008). An extended transcriptional network for pluripotency of embryonic stem cells. Cell *132*, 1049–1061.

Kim, J., Cantor, A.B., Orkin, S.H., and Wang, J. (2009). Use of in vivo biotinylation to study protein-protein and protein-DNA interactions in mouse embryonic stem cells. Nat. Protoc. *4*, 506–517.

Kim, J., Woo, A.J., Chu, J., Snow, J.W., Fujiwara, Y., Kim, C.G., Cantor, A.B., and Orkin, S.H. (2010). A Myc network accounts for similarities between embryonic stem and cancer cell transcription programs. Cell *143*, 313–324.

Lee, T.I., Jenner, R.G., Boyer, L.A., Guenther, M.G., Levine, S.S., Kumar, R.M., Chevalier, B., Johnstone, S.E., Cole, M.F., Isono, K.-I., et al. (2006). Control of developmental regulators by Polycomb in human embryonic stem cells. Cell *125*, 301–313.

Loh, Y.H., Zhang, W., Chen, X., George, J., and Ng, H.H. (2007). Jmjd1a and Jmjd2c histone H3 Lys 9 demethylases regulate self-renewal in embryonic stem cells. Genes Dev. *21*, 2545–2557.

Margueron, R., and Reinberg, D. (2011). The Polycomb complex PRC2 and its mark in life. Nature *469*, 343–349.

Meshorer, E., and Misteli, T. (2006). Chromatin in pluripotent embryonic stem cells and differentiation. Nat. Rev. Mol. Cell Biol. *7*, 540–546.

Min, I.M., Waterfall, J.J., Core, L.J., Munroe, R.J., Schimenti, J., and Lis, J.T. (2011). Regulating RNA polymerase pausing and transcription elongation in embryonic stem cells. Genes Dev. *25*, 742–754.

Mosammaparast, N., and Shi, Y. (2010). Reversal of histone methylation: biochemical and molecular mechanisms of histone demethylases. Annu. Rev. Biochem. *79*, 155–179.

Nechaev, S., and Adelman, K. (2011). Pol II waiting in the starting gates: regulating the transition from transcription initiation into productive elongation. Biochim. Biophys. Acta *1809*, 34–45.

Orkin, S.H., and Hochedlinger, K. (2011). Chromatin connections to pluripotency and cellular reprogramming. Cell *145*, 835–850.

Pedersen, M.T., and Helin, K. (2010). Histone demethylases in development and disease. Trends Cell Biol. *20*, 662–671.

Peterlin, B.M., and Price, D.H. (2006). Controlling the elongation phase of transcription with P-TEFb. Mol. Cell *23*, 297–305.

Rahl, P.B., Lin, C.Y., Seila, A.C., Flynn, R.A., McCuine, S., Burge, C.B., Sharp, P.A., and Young, R.A. (2010). c-Myc regulates transcriptional pause release. Cell *141*, 432–445.

Shao, Z., Zhang, Y., Yuan, G.-C., Orkin, S.H., and Waxman, D.J. (2012). MAnorm: a robust model for quantitative comparison of ChIP-seq data sets. Genome Biol. *13*, R16.

Shi, L., Sun, L., Li, Q., Liang, J., Yu, W., Yi, X., Yang, X., Li, Y., Han, X., Zhang, Y., et al. (2011). Histone demethylase JMJD2B coordinates H3K4/H3K9 methylation and promotes hormonally responsive breast carcinogenesis. Proc. Natl. Acad. Sci. USA *108*, 7541–7546.

Soufi, A., Donahue, G., and Zaret, K.S. (2012). Facilitators and impediments of the pluripotency reprogramming factors' initial engagement with the genome. Cell *151*, 994–1004.

Sridharan, R., Tchieu, J., Mason, M.J., Yachechko, R., Kuoy, E., Horvath, S., Zhou, Q., and Plath, K. (2009). Role of the murine reprogramming factors in the induction of pluripotency. Cell *136*, 364–377.

Takahashi, K., and Yamanaka, S. (2006). Induction of pluripotent stem cells from mouse embryonic and adult fibroblast cultures by defined factors. Cell *126*, 663–676.

Xie, L., Pelz, C., Wang, W., Bashar, A., Varlamova, O., Shadle, S., and Impey, S. (2011). KDM5B regulates embryonic stem cell self-renewal and represses cryptic intragenic transcription. EMBO J. *30*, 1473–1484.

Young, R.A. (2011). Control of the embryonic stem cell state. Cell *144*, 940–954.

Zhang, Y., Liu, T., Meyer, C.A., Eeckhoute, J., Johnson, D.S., Bernstein, B.E., Nusbaum, C., Myers, R.M., Brown, M., Li, W., and Liu, X.S. (2008). Model-based analysis of ChIP-seq (MACS). Genome Biol. *9*, R137.

Zhou, V.W., Goren, A., and Bernstein, B.E. (2011). Charting histone modifications and the functional organization of mammalian genomes. Nat. Rev. Genet. *12*, 7–18.